

Research article

Optimizing interfacial interactions between functionalized graphene and chitosan for enhanced strength and toughness of composite films

Tengxin Zhang^{1,2}, Han Wang^{1,2}, Yabin Hao^{1,2}, Chang Liu^{1,2}, Yan Zhao³, You Zeng^{1,2*}

¹Shenyang National Laboratory for Materials Science, Institute of Metal Research, Chinese Academy of Sciences, 110016 Shenyang, P. R. China;

²School of Materials Science and Engineering, University of Science and Technology of China, 110016 Shenyang, P.R. China

³Ji Hua Laboratory, 528200 Foshan, P. R. China

Received 3 May 2022; accepted in revised form 25 August 2022

Abstract. Remarkable mechanical reinforcement of chitosan films using graphene is extremely important to greatly widen the practical application of chitosan (CS) in many fields, but there still exist challenges to regulating graphene-CS interactions for both enhanced strength and toughness. In this work, we functionalized graphene oxide (GO) with carboxyl (G-COOH) and amino groups (G-NH₂), and investigated the effects of interfacial interactions on the mechanical properties of graphene/CS composite films in detail. We found that the G-NH₂/CS composites exhibited the most remarkable reinforcement in both tensile strength and toughness than the GO/CS and G-COOH/CS composites, even different from a theoretical prediction on graphene-CS interactions. Such remarkable reinforcement is mainly attributed to the moderate graphene-CS interaction, uniform dispersion, and high alignment of G-NH₂ in CS films.

Keywords: nanocomposites, polymer composites, mechanical properties, graphene, interfacial interaction

1. Introduction

Chitosan (CS) is one of the most abundant natural macromolecules on the earth [1–3], and it has been widely used as a multi-functional film in the fields of food packaging, water treatment, and biomedical materials because of its good biocompatibility, bacterial resistance, adsorption capability, and biological degradability [4–7]. However, CS films generally possess unsatisfactory mechanical strength due to weak intermolecular interactions, which cannot meet gradually-increasing requirements of high strength and toughness for high-performance films such as medical bandages, wound dressing, and packaging materials [8, 9]. Recently, many methods of chemical cross-linkage, graft copolymerization, and functionalized

modification have been developed to improve the mechanical performance of CS films [10–12], but these chemical synthesis processes are rather complicated and time-consuming [13]. By contrast, directly adding nanofillers into the CS matrix has been proved to be an effective method for mechanical reinforcement in a simple way [14, 15].

For the achievement of remarkable mechanical reinforcement, high-level dispersion and strong nanofiller-CS interactions are two critical influencing factors [14]. It has been reported that nanofillers such as clay, montmorillonite, zeolite, and carbon nanotubes (CNTs) can be used to effectively improve the mechanical strength of CS matrix, but there still exist some problems of poor dispersion, severe aggregation,

*Corresponding author, e-mail: yuzeng@imr.ac.cn

© BME-PT

or entanglement of CNTs, resulting in unsatisfactory mechanical reinforcement [16, 17]. Graphene possesses unique two-dimensional graphitic structures, excellent mechanical performance, low density, and large diameter/thickness ratio, making it much easier to be well dispersed throughout the matrix than the entangled CNTs [18–20]. In addition, graphene can be further chemically modified to graft various chemical functional groups for forming good compatibility and strong interfacial interactions with CS [21, 22]. Graphene oxide (GO), as one derivative of graphene, possesses plenty of oxygen-containing functional groups to form strong interactions with CS through electrostatic attraction and hydrogen bonding [23, 24], greatly improving tensile strength and Young's modulus of CS films. Furthermore, grafting functional groups onto GO can effectively regulate interfacial interactions between graphene and CS for desired mechanical reinforcement [23, 25, 26]. Huang *et al.* [27] have prepared tea polyphenol-modified GO (TPG) and obtained TPG/CS composite films with improved mechanical strength due to homogeneous dispersion and strong interfacial interactions. In addition, trimethyl silane, phosphoric acid, and sulfonic acid have been grafted onto GO surfaces to increase the mechanical strength of CS films [28, 29]. On the other hand, graphene orientation, similar to biomimetic nacre structures, is also beneficial to realizing enhancement in both tensile strength and toughness of CS films [30, 31]. Although mechanical reinforcement of graphene/CS composites has been widely investigated, the intrinsic reinforcement mechanism based on graphene-CS interactions has not been clearly demonstrated. Zhang *et al.* [25] have theoretically calculated interaction energy between functionalized graphene (FG) and CS and reported that carboxyl groups of FG were much more beneficial to forming strong interfacial interactions with CS for remarkable reinforcement than hydroxyl and amino groups. It is worth pointing out that the ultimate mechanical properties of graphene/CS composites depend on not only the graphene-CS interactions but also the microstructures of composites. There still exist challenges to regulate graphene-CS interactions and microstructures for the high tensile strength and toughness of graphene/CS composites.

This work aims to fabricate high-performance graphene/CS composite films with high strength and toughness. It is the first time to clearly clarify interfacial interactions between functionalized graphene

(FG) and CS and to build a relationship of interfacial interactions with microstructures and ultimate mechanical properties for the fabrication of high-performance composites. We used GO as a precursor and prepared functionalized graphene with carboxyl groups (G-COOH) or amino groups (G-NH₂). Dispersion stability and rheological behavior of FG/CS solutions were measured to evaluate FG-CS interactions. The FG/CS composite films were fabricated using a solution-casting method, and their microstructures and mechanical properties were investigated in detail to establish a relationship between FG-CS interactions with mechanical reinforcement. We found that the G-COOH could form the strongest interactions with CS than the GO and G-NH₂ as theoretical prediction, but the G-NH₂/CS composites exhibited the highest tensile strength and toughness among all the composites. It reveals that the interfacial interaction plays an important role in greatly influencing the dispersion stability of FG/CS solutions, but the ultimate performance of FG/CS composites strongly depends on the microstructure and FG alignment. Comprehensive consideration of both interfacial interactions and resultant microstructures is extremely essential to designing and fabricating high-performance graphene/CS composite films with enhanced strength and toughness.

2. Experimental

2.1. Materials

Chitosan (CS, deacetylation degree of 88%, $M_w = 8000\text{--}20000$) was obtained from Sinopharm Chemical Reagent Co. Ltd in China. Graphene oxide (GO) was purchased from Sixth Element Materials Technology Co. Ltd. (Changzhou, China), and its layer numbers and lateral size were less than 10 graphitic layers and 5–15 μm , respectively. The GO possessed plenty of oxygen-containing functional groups, showing good aqueous dispersibility and high chemical activity. Analytic reagents of 65% nitric acid, 98% sulfuric acid, ethylenediamine (EDA), dimethylformamide (DMF), and glacial acetic acid were purchased from Sinopharm Chemical Reagent Co. Ltd. in China.

2.2. Synthesis of functionalized graphene

GO was used as a precursor to prepare functionalized graphene with carboxyl or amino groups. Carboxyl-functionalized graphene (G-COOH) was prepared as follows [32]: GO of 100 mg was weighed

and poured into a 40 ml mixed acid solution of HNO₃ and H₂SO₄ (volume ratio of 1:3). The GO-containing suspension was heated up to 80 °C and refluxed for 8 h. With the increment of carboxyl groups, the GO was further chemically oxidized into G-COOH. Thereafter, the obtained suspension was diluted and repeatedly washed with deionized water to remove residuals. After being freeze-dried at –55 °C for 24 h, G-COOH nanosheets were prepared. As for the preparation of amino-functionalized graphene (G-NH₂), 80 mg GO was put into 40 ml DMF and ultrasonically treated for 30 min, then 1.5 ml EDA was added to chemically react with GO in a sealed vessel at 80 °C for 8 h. The EDA could react with GO through nucleophilic substitution and amidation reaction, consequently introducing amino groups onto GO and obtaining G-NH₂ [33]. Thereafter, the G-NH₂-containing suspension was vacuum-filtrated and repeatedly washed out with deionized water for the removal of residuals. After freeze-drying at –55 °C for 24 h, G-NH₂ nanosheets were obtained.

2.3. Fabrication of FG/CS composite films

The GO, G-COOH, and G-NH₂ were weighed respectively and dispersed ultrasonically in deionized water to prepare 2 mg/ml FG suspensions. The obtained suspensions were poured into 2 wt% chitosan solutions which were prepared by dissolving chitosan into 1 vol% acetic acid solutions. The mixtures were mechanically stirred for 4 h to obtain a homogeneous dispersion of FG. Thereafter, the FG/CS mixtures were cast into plastic Petri dishes and dried in an oven at 37 °C for 48 h. As a result, FG/CS composite films with 1.5 wt% FG loadings and 0.06 mm thickness were obtained.

2.4. Characterization

Fourier transform infrared (FT-IR) and X-ray photoelectron (XPS) spectra of samples were recorded on Bruker Tensor 27 (Germany) and Escalab 250 (Thermo Scientific, USA), respectively for analyzing functional groups and elemental compositions. Raman spectra were measured to evaluate the structural integrity of samples by using Jobin Yvon LabRam HR800 (Horiba, France). An X-ray diffractometer (XRD, D/max 2400 with Cu K_α radiation, Japan) was used to characterize the crystalline structures of the samples. Optical microscopic images of FG/CS solutions were observed using Nikon Eclipse

LV100ND (Japan) at room temperature for evaluation of dispersion stability. Surface charges of FG in aqueous and CS solutions were measured using a Zeta potential analyzer (Malvern Zetasizer Nano-ZS90, UK). Particle size distribution of the FG and FG/CS clusters in aqueous solutions was measured using a laser particle size analyzer (Malvern Mastersizer 2000, UK). Microstructures of FG/CS composite films were observed using a scanning electron microscope (SEM, NavoSEM430, FEI, USA) at 10 kV.

2.5. Performance testing

The rheological behavior of FG/CS solutions was measured using a Pin's viscometer and a rotational rheometer (Haake Mars II, USA) equipped with a cone-partitioned plate fixture at shear rates ranging from 0.1 to 10 s⁻¹. Thermogravimetric analysis (TGA) was conducted on Netzsch STA-499C (Germany) at a heating rate of 10 °C/min from 30 to 700 °C in an argon atmosphere to evaluate the effect of FG-CS interactions on the thermal stability of composites. Mechanical properties of composite films were measured with a dynamic mechanical analyzer (DMA Q800, TA Instrument, USA) in a tensile mode at a force-loading speed of 1 N/min at room temperature, and the specimen size was 40 mm × 3 mm × 0.06 mm.

3. Results and discussion

3.1. Preparation and characterization of functionalized graphene

Functionalized graphene with carboxyl or amino groups was prepared using GO as a precursor. The preparation mechanism and chemical compositions of the GO, G-COOH, and G-NH₂ were shown in Figure 1. As shown in Figure 1a, the GO prepared by Hummers' method possesses numerous hydroxyl, epoxy, and carboxyl groups, and they can be easily modified into various functionalized graphene [34]. In this work, the G-COOH was prepared by chemically oxidizing GO with increased contents of carboxyl groups [35], and the G-NH₂ was obtained through nucleophilic substitution and amidation reaction between GO and EDA [33]. These above-mentioned reactions are mild and easily operated without severely destroying graphitic structures of GO, and all the FG show a similar particle size distribution in Figure 1b. The changes in functional groups before and after modification can be confirmed from FT-IR analysis (see Figure 1c). The GO shows characteristic peaks at 1720, 1230, and 1050 cm⁻¹, corresponding

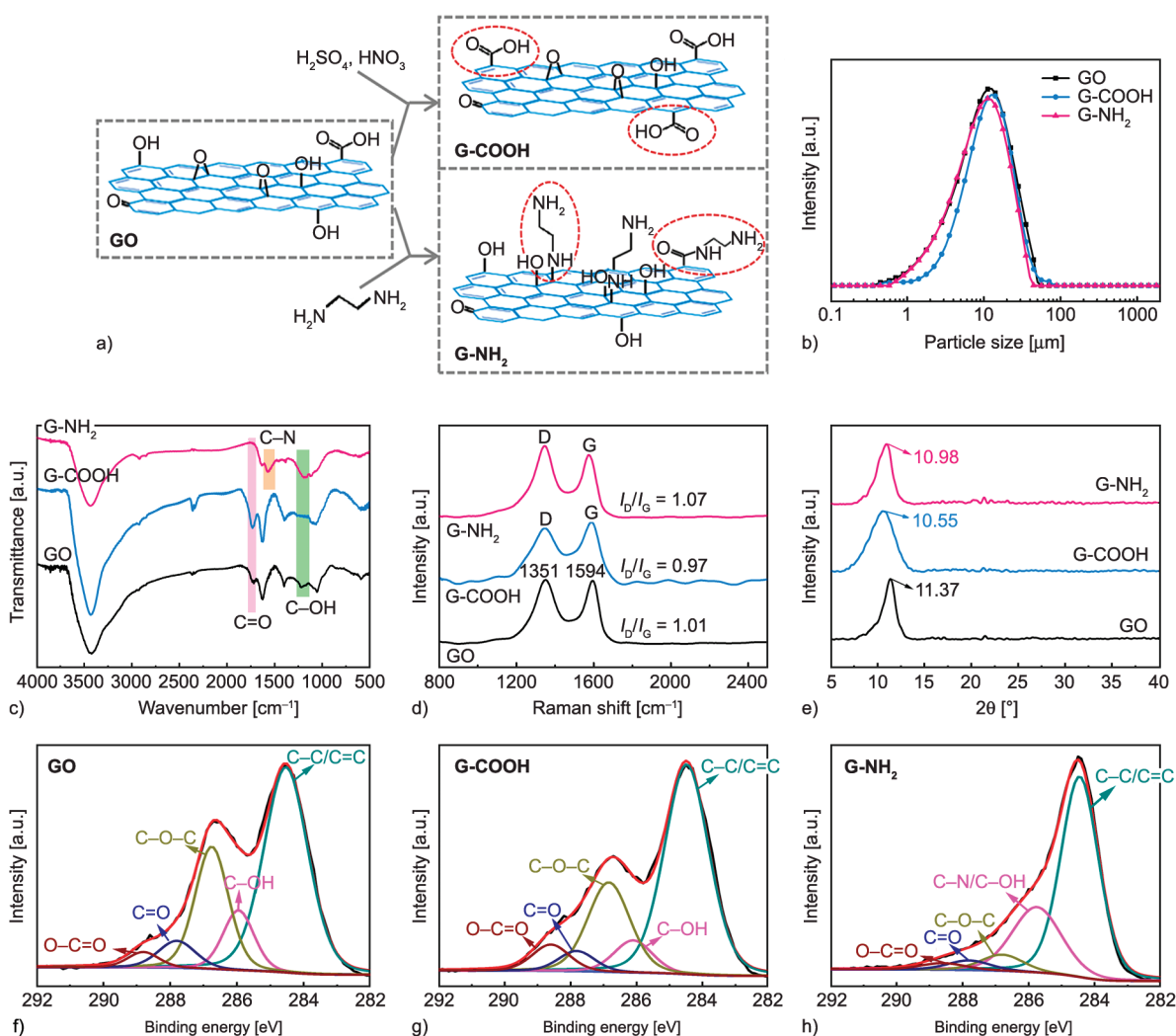


Figure 1. (a) Preparation schematic of functionalized graphene with carboxyl and amino groups. (b) Particle size distribution, (c) FT-IR spectra, (d) Raman spectra, (e) XRD patterns, and (f–h) C1s XPS spectra of the GO, G-COOH, and G-NH₂.

to stretching vibrations of C=O from COOH, C–OH, and C–O–C, respectively [36, 37]. The G-COOH exhibits an enhanced relative intensity at 1720 cm⁻¹ and a weakened vibration peak at 1230 cm⁻¹, revealing that the C–OH was chemically oxidized into COOH [36]. For the G-NH₂, its characteristic peaks at 1720 and 1050 cm⁻¹ were weakened with increased intensities at 1564 and 1230 cm⁻¹, implying that the amino groups were covalently grafted onto GO nanosheets [33].

Microstructures of the FG were determined by Raman and XRD (see Figures 1d–1e). It can be seen that all the FG show Raman characteristic peaks with D and G bands at 1351 and 1594 cm⁻¹, and similar XRD diffraction peaks at about 11°, implying that the chemical modification has not severely destroyed the graphitic structures of graphene. We can still find slight changes in the intensity ratio of the D band to G band (I_D/I_G) due to the introduction of edge defects

during modification [38]. In addition, slight shifts of the diffraction peak towards low degree after modification indicate enlarged lamellar spacing from lamellar repulsion and steric hindrance caused by carboxyl and amino groups [39]. Figures 1f–1h show XPS spectra of FG for the characterization of chemical compositions. The increased intensities of the O–C=O peak at 288.6 eV for G-COOH and the C–N peak at 285.8 eV for G-NH₂ also confirm the presence of carboxyl and amino groups [37], which is consistent with the FT-IR analysis. Therefore, the functionalized graphene with carboxyl or amino groups was obtained by chemical modification without severely destroying the microstructure of graphene.

3.2. Dispersion of FG in CS solutions

These FG with various functional groups can form different interactions with CS, greatly influencing the dispersion of FG in CS solutions. Figure 2 shows

dispersion stability, surface charge (zeta potential), and size distribution of FG/CS solutions. It can be seen from Figure 2a that the GO, G-COOH, and G-NH₂ show distinct dispersion stability in CS solutions after 12 h settlement. The G-COOH exhibits the poorest stability in the CS solution accompanied by obvious aggregation, while the GO and G-NH₂ show satisfactory dispersion stability. Such phenomena can also be observed from optical microscopic images in Figures 2b–2e. We can see several aggregations of large-size clusters in the G-COOH/CS solution, followed by the GO/CS solution. By contrast, the G-NH₂ shows homogenous dispersion in the CS solution without apparent aggregation. Notably, all these FG possess nearly the same particle size and distribution shown in Figure 1b, but they exhibit distinct aggregation and particle sizes in CS solutions, which is closely associated with interfacial interactions of FG with CS.

We measured the Zeta potentials of the CS, FG, and FG/CS solutions for elucidation of the surface charges and FG-CS interactions (see Figure 2f). We can see that the CS exhibits a typical positive-charge characteristic with a Zeta potential of 66.6 mV due to amine protonation of CS in weak acid conditions [40]. The GO and G-COOH show negative surface charges with Zeta potentials of -40.9 and -54.8 mV in the presence of carboxyl groups respectively, while the G-NH₂ exhibits typical positive surface charges with a 14.2 mV potential. These diverse surface charges of FG can form distinct interactions with positive-charge CS. First of all, the G-COOH possesses plenty of carboxyl groups and exhibits much more negative charges than the GO, and it can form stronger interactions with CS through electrostatic attraction. By contrast, the G-NH₂ shows the same positive charges with CS, and its interactions with CS are much lower than that of the G-COOH and GO. Notably, we can

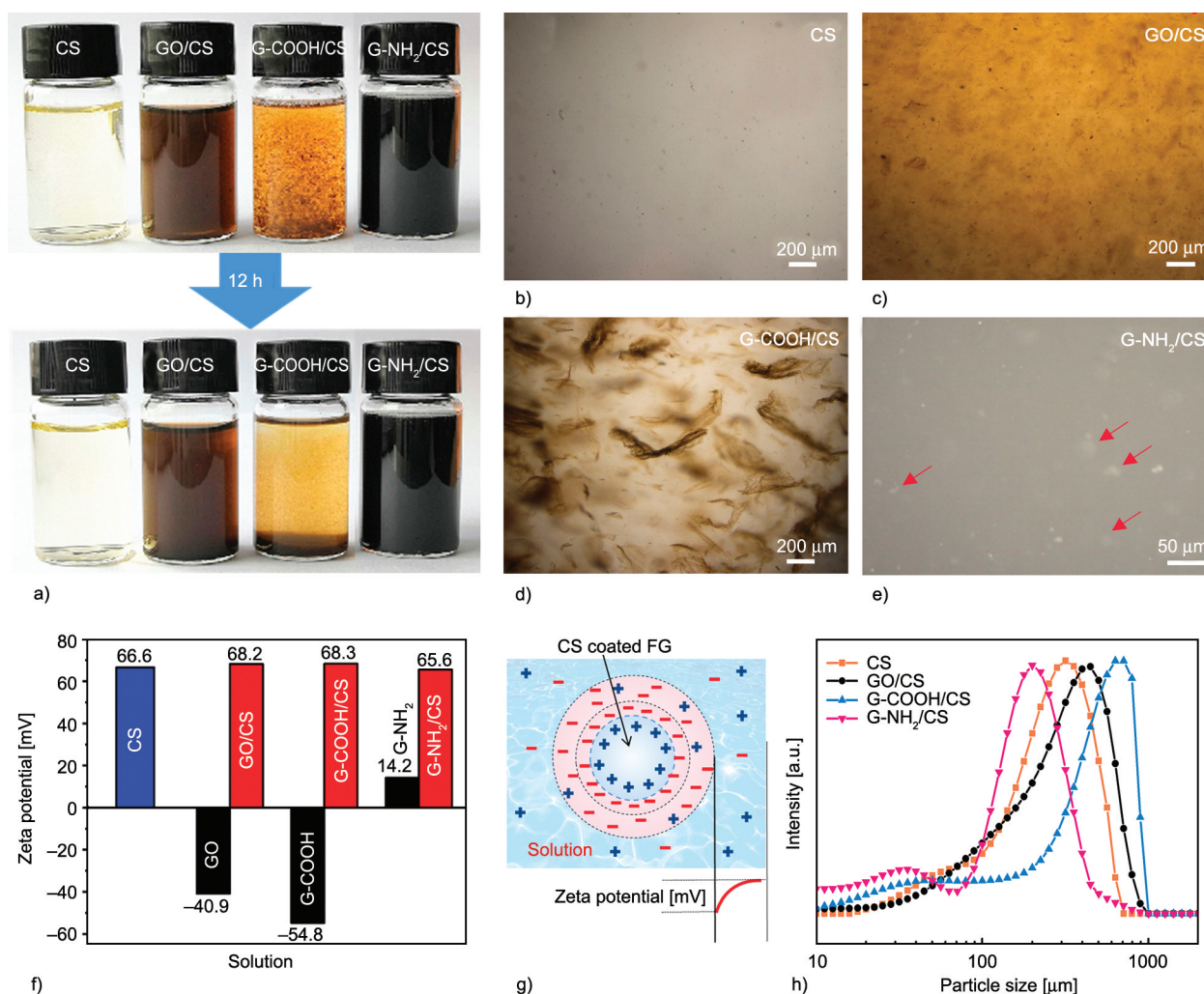


Figure 2. (a) Dispersion stability of FG/CS solutions. Optical micrographs of the (b) CS, (c) GO/CS, (d) G-COOH/CS, (e) G-NH₂/CS solutions. (f) Zeta potentials of the FG and FG/CS solutions. (g) Schematic of surface charges of FG in CS solutions. (h) Particle size distribution of the CS and FG/CS solutions.

see in Figure 2f that all the FG/CS solutions exhibit nearly the same potential of about 67 mV as the CS solution, implying that the FG surfaces were covered with positive-charge CS. It is because the FG possesses high surface energy and spontaneously adsorb CS onto its surfaces for charge balance, as shown in Figure 2g, resulting in the formation of CS-coated FG clusters and resultant positive Zeta potentials.

We further measured the particle size distribution of FG/CS solutions using a laser particle size analyzer (see Figure 2h). It can be seen clearly that the G-COOH/CS exhibits the largest average particle size of about 700 μm , much higher than that for the GO/CS and G-NH₂/CS. The G-COOH possesses plenty of negative surface charges, and it can form extremely strong interactions with CS and adsorb much more CS onto G-COOH surfaces, resulting in the formation of large-size GOOH/CS clusters, severe aggregation, and poor dispersion stability (see Figure 2d). Compared with the G-COOH/CS solution, the GO/CS solution exhibits a smaller cluster size and better dispersion stability due to the weaker interactions. For the G-NH₂ with positive surface charges, it can form the weakest interactions with CS, consequently resulting in the smallest size of clusters and the best dispersion stability. Therefore, the FG with various functional groups can form distinct interactions with CS, strongly influencing the aggregation and dispersion stability of FG/CS solutions.

3.3. Rheological behavior of FG/CS solutions

We measured the rheological behavior of FG/CS solutions to investigate the effect of FG-CS interactions on solution viscosity, as shown in Figure 3. It can be seen from Figure 3a that all the FG/CS solutions exhibit higher dynamic viscosity than the CS solution, indicating that the presence of FG can result in increased viscosity by hindering the motion of CS chains to some extent. Among all the FG/CS solutions, the G-NH₂/CS solution exhibits the lowest viscosity, followed by the G-COOH and GO/CS solutions. Such the same tendency can also be observed from kinematic viscosity measured using Pin's viscometers (see Figure 3b). The viscosity of fluid generally reflects the resistance to gradual deformation by shear or tensile stress, which is closely associated with inter-molecular friction and interactions between particles [8]. Figure 3c illustrates the FG-CS interactions and FG aggregation (FG/CS cluster) in CS solutions. As mentioned above, the GO and

G-COOH with negative charges can form strong electrostatic attractions with the CS and result in the formation of large-size clusters, consequently causing increased friction resistance and high viscosity. By contrast, the G-NH₂ with positive charges possesses moderate interactions with CS, and they can form small-size G-NH₂/CS clusters, resulting in decreased resistance and low viscosity for high dispersion stability. Therefore, the rheological behavior of FG/CS solutions strongly depends on the FG-CS interaction, friction resistance, and cluster size. The low viscosity of G-NH₂/CS solutions is beneficial to realizing homogenous dispersion and high orientation of the G-NH₂ in the CS matrix for remarkable mechanical reinforcement.

3.4. Fabrication and microstructures of FG/CS composite films

The FG/CS composite films were prepared using the solution-casting technique, and their SEM images are shown in Figure 4. In comparison with smooth fracture surfaces of the CS film, the FG/CS composites exhibit coarse and rough surfaces, and some FG aggregation can be observed. Among all the composites, the G-COOH/CS composites show the most severe aggregation in Figure 4c, mainly attributed to the large size of G-COOH/CS clusters and inhomogeneous dispersion. By contrast, the GO/CS and G-NH₂/CS composites show homogenous dispersion due to their small-size clusters and slight aggregation. Notably, we can see highly-aligned G-NH₂ in CS matrix along in-plane directions (see Figure 4d), which is closely associated with the high motion ability of the small-size clusters. During the fabrication of composite films, the G-NH₂ can be easily dispersed and aligned along the in-plane direction under interlaminar shearing forces. Such alignment of G-NH₂ in CS matrix is beneficial to improving both strength and toughness of composite films.

3.5. Interfacial interactions and thermal stability of FG/CS composites

Interfacial interactions between FG and CS in composite films were characterized using FT-IR and Raman techniques, as shown in Figure 5. It can be seen from Figure 5a that the CS films show typical characteristic peaks at 1630, 1402, and 1560 cm^{-1} , corresponding to vibrations of the C=O from amide I, C–N from amide III, and the N–H bending, respectively [41]. After adding GO into CS films, the adsorption

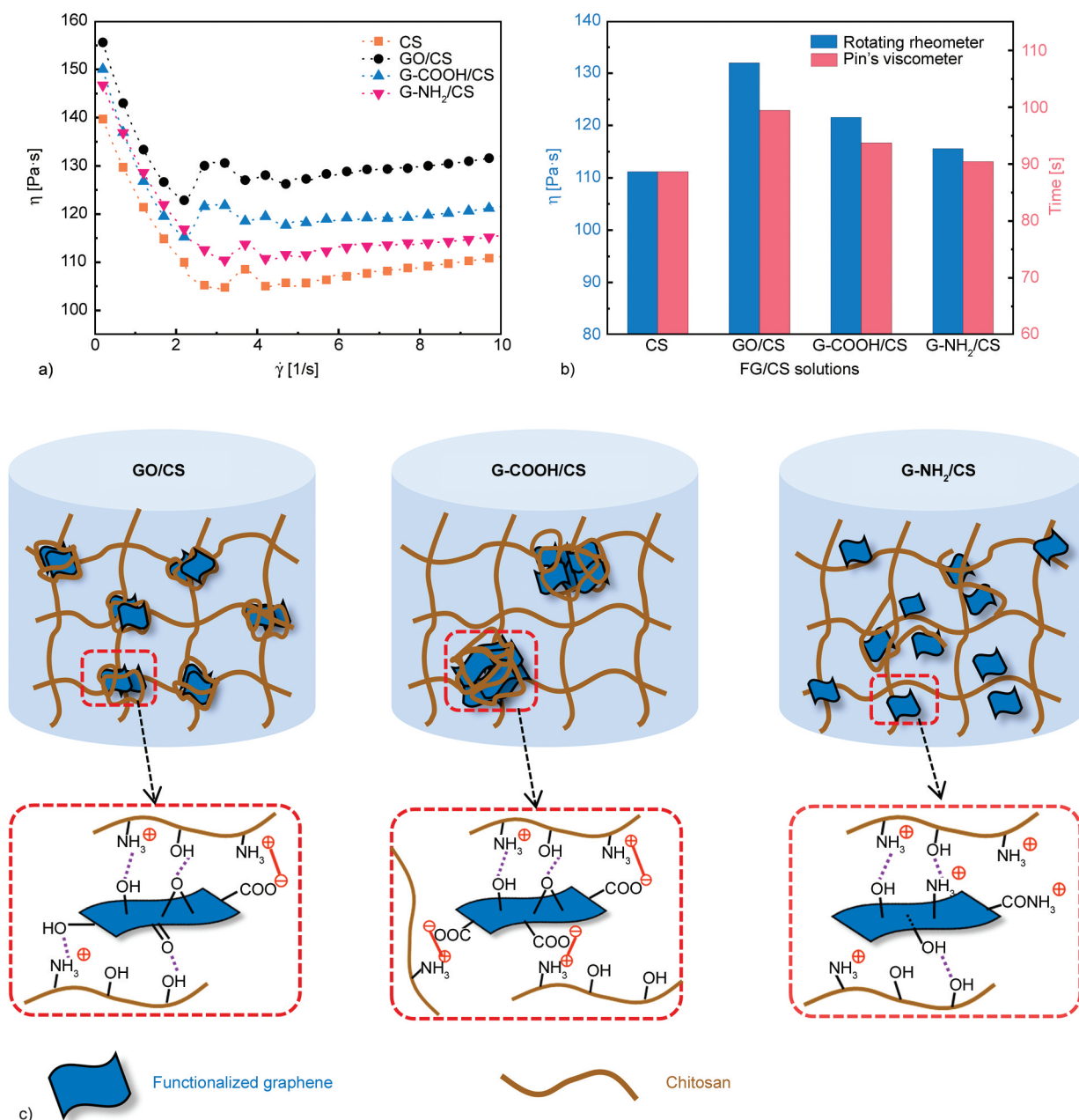


Figure 3. Viscosity of FG/CS solutions measured using (a) rotational rheometer and (b) Pin's viscometer. (c) Schematics of interaction and aggregation of the GO/CS, G-COOH/CS, and G-NH₂/CS solutions.

bands for C=O and C–N shift to 1635 and 1397 cm⁻¹, respectively, more susceptible to that for N–H, which is consistent with that reported in the literature [41, 42]. These shifts of characteristic peaks are mainly attributed to the graphene-CS interactions through hydrogen bonds and electrostatic attractions. In our work, the G-COOH/CS composites exhibit the largest shift, followed by the GO/CS and G-NH₂/CS, indicating that the G-COOH can form stronger interactions with CS than the GO and G-NH₂. Such strong interactions can also be confirmed through Raman analysis shown in Figure 5b. The G-COOH/CS composites exhibit the I_D/I_G value of 1.05, higher

than 0.97 for the corresponding G-COOH shown in Figure 1d. Such increased values imply additional defects caused by electrostatic attractions with CS [43]. In our work, the G-COOH/CS composites exhibit the largest I_D/I_G increment than the GO/CS and G-NH₂/CS composites, revealing that the G-COOH can form the strongest interactions with CS, followed by the GO and G-NH₂.

The thermal stability of the FG/CS composites was investigated and shown in Figures 5c–5d. It can be seen that all the FG/CS composites exhibit higher thermal stability than the CS because the presence of FG can effectively hinder the motion of CS chains at

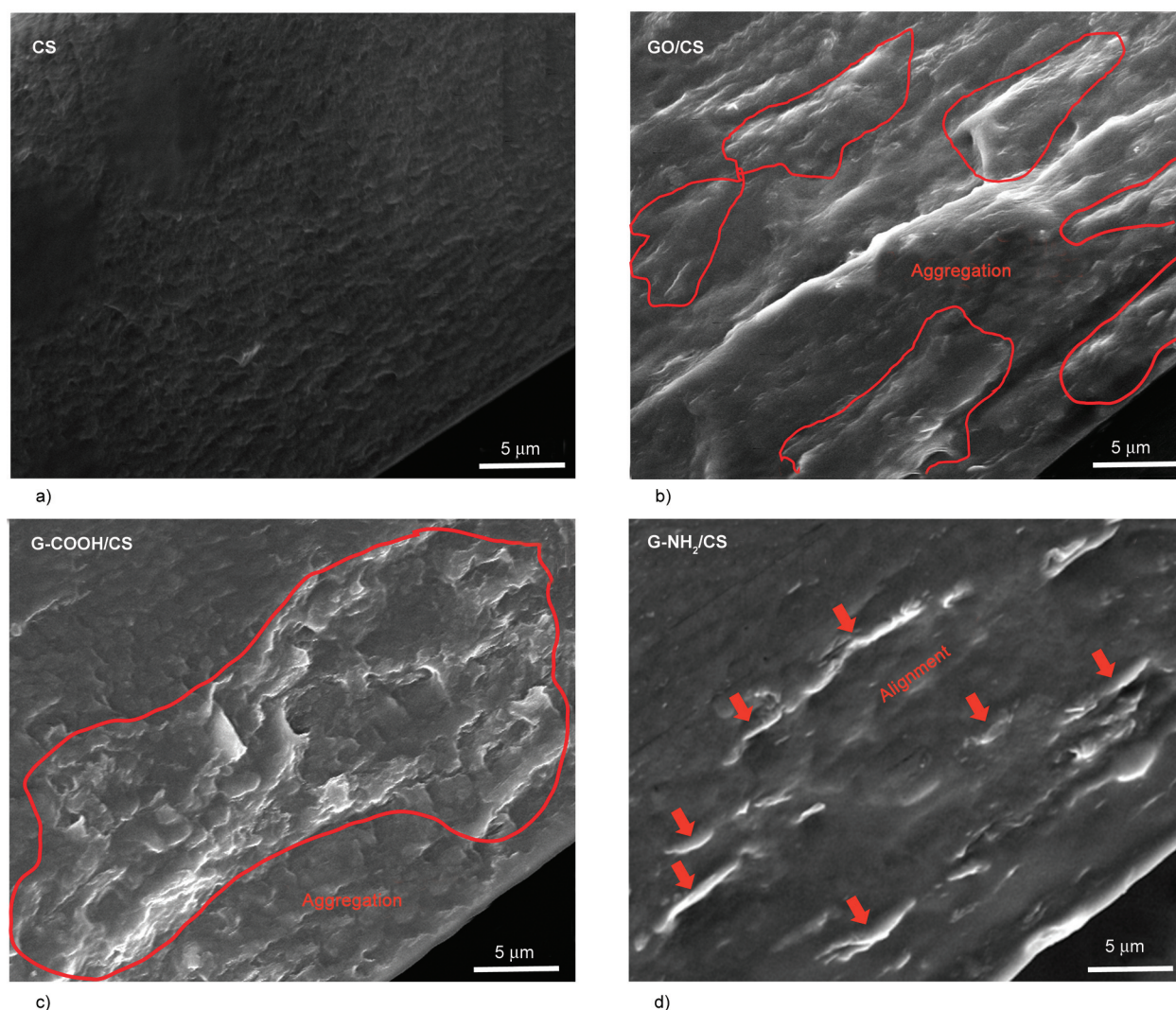


Figure 4. SEM images of (a) the CS, (b) GO/CS, (c) G-COOH/CS, and (d) G-NH₂/CS composite films.

elevated temperatures. Among all the FG/CS composites, the GO/CS and G-COOH/CS composites show higher thermal stability than the G-NH₂/CS composites because of their stronger interactions with CS. Notably, the GO/CS composites show much higher stability than the G-COOH/CS composites, although the GO possesses weaker interactions with CS than the G-COOH. It is mainly attributed to the better dispersion of GO in CS matrix (see Figure 4), effectively restricting CS chain motions and resulting in high thermal stability of composites [41]. Therefore, the FG/CS composites exhibit improved thermal stability of CS, which is closely associated with strong interfacial interactions.

3.6. Mechanical properties of FG/CS composite films

Tensile properties of the FG/CS composites were measured to evaluate the reinforcing effect of the FG with various functional groups, as shown in Figure 6.

It can be seen from Figure 6a that the G-NH₂/CS and GO/CS composites exhibit much higher tensile strength and elastic modulus (slopes of the initial linear region) than the CS, indicating that the presence of FG can significantly enhance the mechanical properties of CS films. As shown in Figure 6b, the tensile strength of the G-NH₂/CS and GO/CS composites is up to 81.8 and 75.8 MPa, respectively, increasing by 24.7 and 15.5% in comparison with 65.6 MPa for the CS films. It is notable that the G-COOH/CS composites show even lower tensile strength than the CS films despite the extremely strong interactions between G-COOH and CS, which is mainly attributed to the poor dispersion of the large-size clusters shown in Figure 4c. In comparison with satisfactory dispersion of the GO and G-NH₂ in the CS matrix, the G-COOH is prone to severely aggregate with CS through excessive interactions and form large-size clusters, consequently resulting in poor dispersion and unsatisfactory reinforcement.

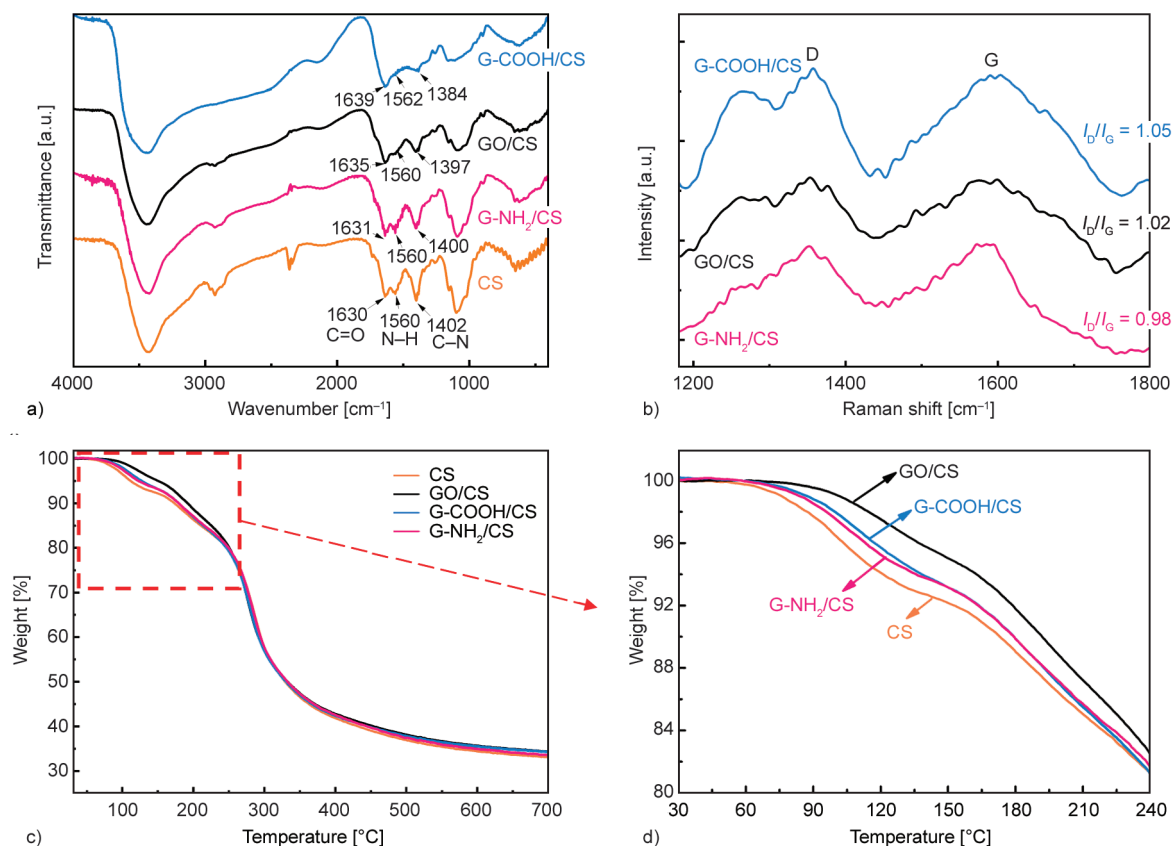


Figure 5. (a) FT-IR and (b) Raman spectra, and (c, d) thermogravimetric curves of FG/CS composite films.

We further compared the elongation at break and tensile toughness of FG/CS composites. It can be seen from Figures 6c–6d that the G-NH₂/CS composites exhibit the maximum elongation at break (22.4%) and highest tensile toughness (16.2 MJ/m³) among all the composites. It means that the presence of G-NH₂ can increase not only the tensile strength but also the tensile toughness of CS. Such remarkable reinforcement is mainly attributed to the uniform dispersion and highly-aligned structure along tensile directions. It has been reported that the alignment of graphene is beneficial to effectively transferring stress and dissipating fracture energy through interfacial friction slipping [31], consequently resulting in enhanced strength and toughness of composites. In our work, the G-NH₂ possesses moderate interactions with CS and forms small-size G-NH₂/CS clusters, and it is much easier to be well dispersed and form highly-aligned structures during the fabrication process. Such high alignment of G-NH₂ plays an important role in greatly improving the tensile strength and toughness of composites. By contrast, the G-COOH/CS and GO/CS composites exhibit even lower elongation at break and tensile toughness than the CS films in spite of their strong FG-CS interactions,

mainly attributed to the unsatisfactory dispersion and random orientation. Therefore, the mechanical reinforcement of FG/CS composites depends on not only the strong interfacial interactions but also the uniform dispersion and aligned microstructures.

We further compared the mechanical reinforcement in our work with that of other graphene/CS composites reported in the literature. It has been reported that graphene can increase tensile strength and elastic modulus of CS, but sacrifice the tensile toughness with reduced elongation at break by 30, 55, 71, 11, and 10% for GO/CS [27], tea polyphenols-GO/CS [44], sulphonated graphene/CS [28], RGO/CS [45], trimethyl silane-GO/CS [29], respectively. In our work, the G-COOH/CS and GO/CS composites also show reduced toughness and elongation at break than the CS films, consistent with that reported in the literature. It is worth pointing out that the 1.5 wt% G-NH₂/CS composites exhibit remarkable reinforcement in both the tensile strength and toughness, respectively increasing by 24.7 and 37.3% in comparison with the CS films. Such remarkable enhancement is mainly attributed to the uniform dispersion and high alignment of G-NH₂ in CS matrix.

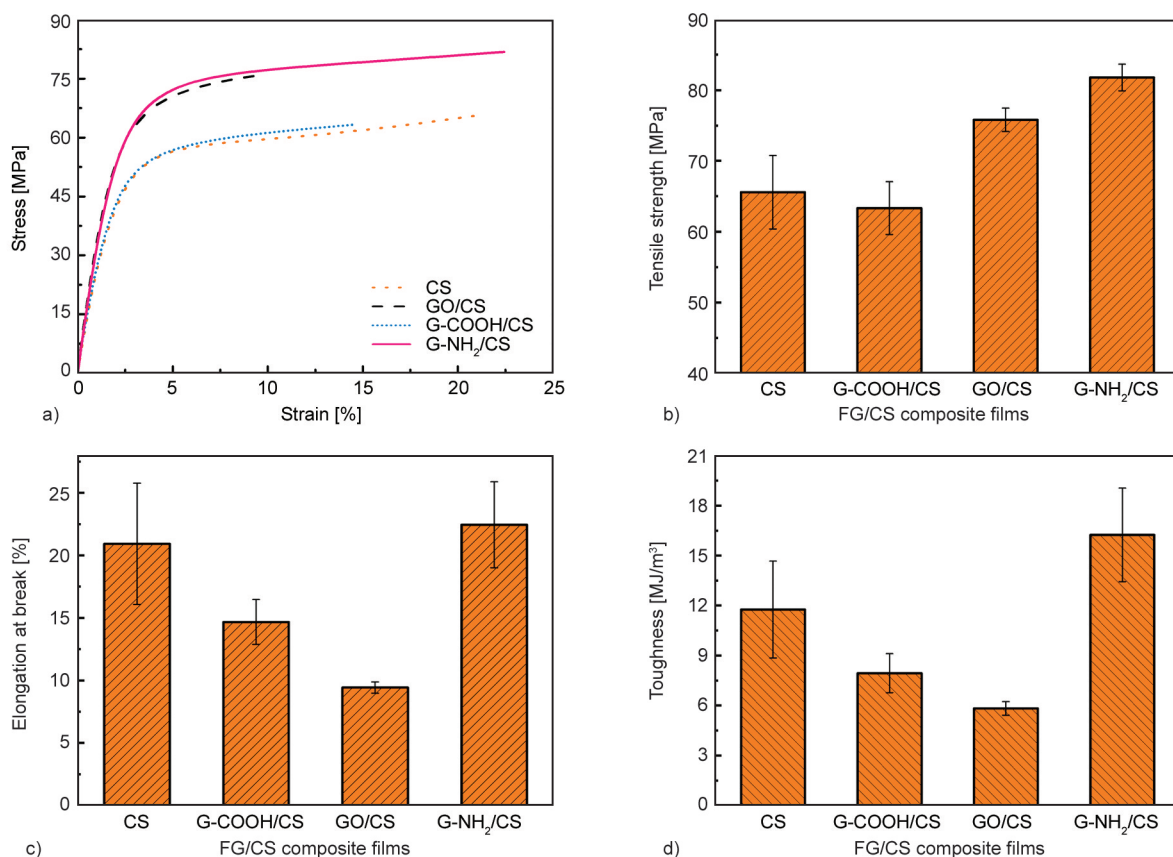


Figure 6. (a) Stress-strain curves, (b) ultimate tensile strength, (c) elongation at break, and (d) tensile toughness of FG/CS composite films.

3.7. Mechanism on improved strength and toughness of FG/CS composites

Figure 7 illustrates the reinforcing mechanism of FG/CS composites. It reveals that the FG with various functional groups can form distinct FG-CS interactions and diverse-size FG/CS clusters, greatly influencing the mechanical strength and toughness of composites. We can see from Figure 7a that the G-COOH can form the strongest interactions with CS as the theoretical prediction but causes severe aggregation, poor dispersion, and decreased mechanical performance (see Figure 7b). For the GO/CS composites, their GO-CS interactions are lower than that of the G-COOH/CS composites, and the GO can be well dispersed throughout the CS matrix, resulting in increased tensile strength (see Figure 7b). Notably, the GO/CS composites still exhibit lower elongation at break, and tensile toughness than the CS, which is because the medium-size GO/CS clusters are still rather difficult to be highly aligned in high-viscosity GO/CS solutions during fabrication. As a result, the random orientation of GO in the CS matrix improves the tensile strength of CS by sacrificing the tensile

toughness, which is consistent with that reported in the literature [8, 27, 44].

As for the G-NH₂/CS composites, the G-NH₂ can form moderate interactions with CS through hydrogen bonds [46], and it can be uniformly dispersed in the CS solution without obvious aggregation. The small-size G-NH₂/CS clusters can be easily aligned in the CS matrix during the fabrication of composite films (see Figure 7a). Such alignment of the G-NH₂ plays an important role in greatly increasing the pulling force of graphene out of the matrix and dissipating fracture energy [31, 47]. Therefore, the G-NH₂/CS composites exhibit remarkable enhancement in tensile strength and toughness, which is mainly attributed to the moderate interfacial interaction, small-size cluster, and high alignment of G-NH₂ in CS matrix. As mentioned above, theoretical calculation predicted that carboxyl groups could form much stronger interfacial interactions with CS than the hydroxyl and amino groups for remarkable mechanical reinforcement [25]. But, in our work, the G-COOH/CS composites exhibit the lowest tensile strength and toughness among all the composites. It

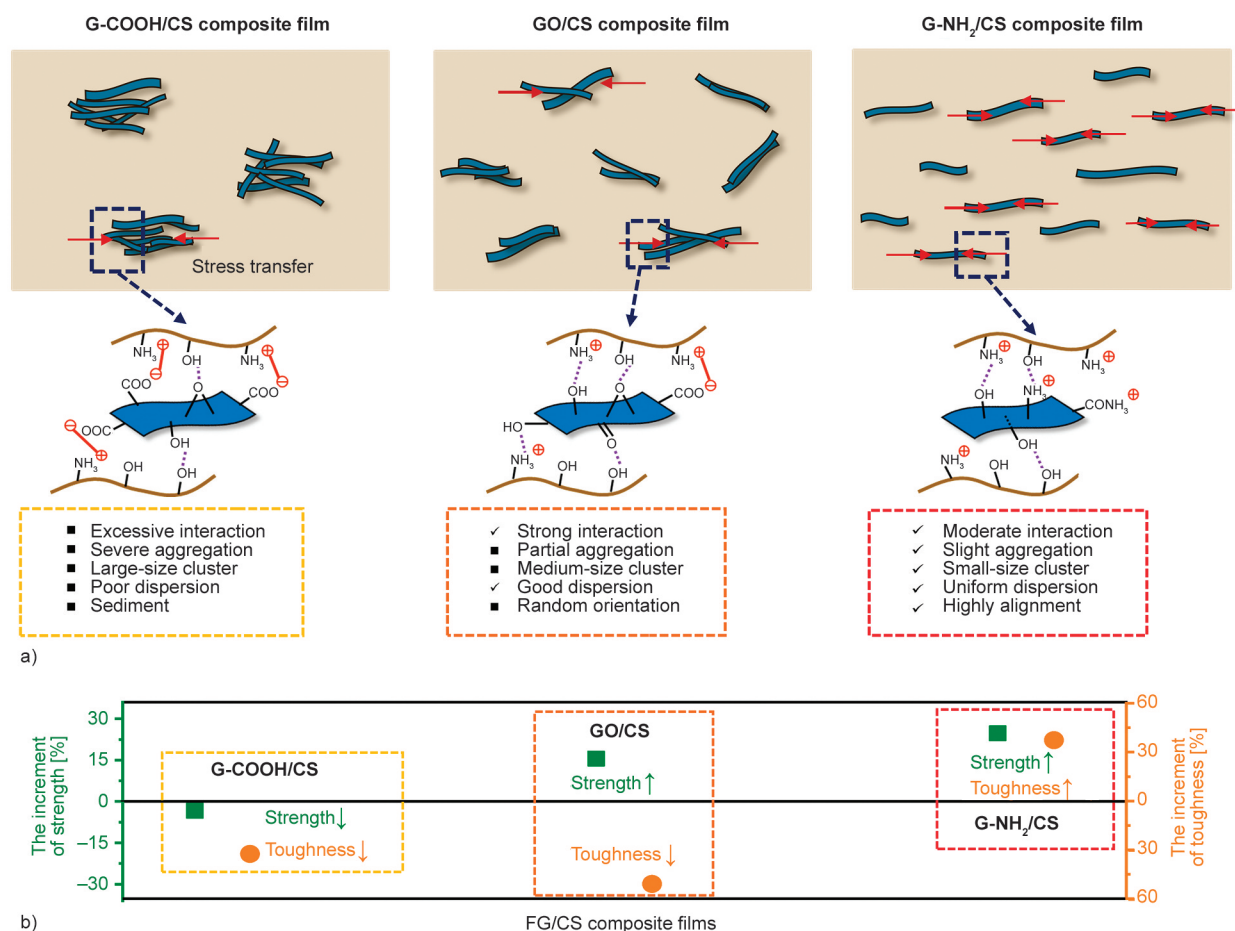


Figure 7. (a) Schematic of FG aggregation based on FG-CS interactions, and (b) the resultant mechanical reinforcement in tensile strength and toughness of FG/CS composites.

indicates that the mechanical reinforcement of graphene/CS composites depends on not only the graphene-CS interactions but also the dispersion stability, rheological behavior, microstructure, and alignment of graphene in the CS matrix. Notably, some influencing factors, such as molecular weight, deacetylation degree, preparation condition, and crystallinity degrees, should be comprehensively considered for the fabrication of high-performance graphene/CS composite films.

4. Conclusions

In this work, the interfacial interactions between CS and functionalized graphene of GO, G-COOH, and G-NH₂ were investigated to clarify the effect of FG-CS interactions on the mechanical properties of FG/CS composite films. The chemical compositions, dispersion stability, rheological behavior, microstructure, thermal stability, tensile strength and toughness of composites were measured in detail. Although theoretical calculation predicted that the G-COOH could form extremely strong interactions with CS for

remarkable mechanical reinforcement, we found that the excessive interactions could inevitably result in severe G-COOH aggregation in solutions, inhomogeneous dispersion, and decreased mechanical performance of composites. By contrast, the G-NH₂/CS composites exhibit remarkable enhancement in both tensile strength and toughness, which is mainly attributed to the moderate interaction, uniform dispersion, and highly-aligned structures. By virtue of their high strength and toughness, the G-NH₂/CS composites show great potential to be used as high-performance films in the field of packaging and biomedical materials.

Acknowledgements

This work was supported by the National Natural Science Foundation of China (Nos. 51802317, 52130209), Liaoning Natural Science Foundation (No. 2019JH3/30100008), and the Opening Foundation of Shanxi Key Laboratory of Nano & Functional Composite Materials (NFCM202102), Shenyang National Laboratory for Materials Science (2021-FP31), and IMR Innovation Fund (2022-PY07).

References

- [1] Pillai C. K. S., Paul W., Sharma C. P.: Chitin and chitosan polymers: Chemistry, solubility and fiber formation. *Progress in Polymer Science*, **34**, 641–678 (2009). <https://doi.org/10.1016/j.progpolymsci.2009.04.001>
- [2] Rinaudo M.: Chitin and chitosan: Properties and applications. *Progress in Polymer Science*, **31**, 603–632 (2006). <https://doi.org/10.1016/j.progpolymsci.2006.06.001>
- [3] Hejazi M., Behzad T., Heidarian P., Nasri-Nasrabadi B.: A study of the effects of acid, plasticizer, cross-linker, and extracted chitin nanofibers on the properties of chitosan biofilm. *Composites Part A: Applied Science and Manufacturing*, **109**, 221–231 (2018). <https://doi.org/10.1016/j.compositesa.2018.02.038>
- [4] Sirajudheen P., Poovathumkuzhi N. C., Vigneshwaran S., Chelaveettil B. M., Meenakshi S.: Applications of chitin and chitosan based biomaterials for the adsorptive removal of textile dyes from water – A comprehensive review. *Carbohydrate Polymers*, **273**, 118604 (2021). <https://doi.org/10.1016/j.carbpol.2021.118604>
- [5] Wang H., Qian J., Ding F.: Emerging chitosan-based films for food packaging applications. *Journal of Agricultural and Food Chemistry*, **66**, 395–413 (2018). <https://doi.org/10.1021/acs.jafc.7b04528>
- [6] Yang S., Lei P., Shan Y., Zhang D.: Preparation and characterization of antibacterial electrospun chitosan/poly(vinyl alcohol)/graphene oxide composite nanofibrous membrane. *Applied Surface Science*, **435**, 832–840 (2018). <https://doi.org/10.1016/j.apsusc.2017.11.191>
- [7] Liu Z., Wang K., Peng X., Zhang L.: Chitosan-based drug delivery systems: Current strategic design and potential application in human hard tissue repair. *European Polymer Journal*, **166**, 110979 (2022). <https://doi.org/10.1016/j.eurpolymj.2021.110979>
- [8] Han D., Yan L., Chen W., Li W.: Preparation of chitosan/graphene oxide composite film with enhanced mechanical strength in the wet state. *Carbohydrate Polymers*, **83**, 653–658 (2011). <https://doi.org/10.1016/j.carbpol.2010.08.038>
- [9] Jayakumar R., Prabakaran M., Kumar P. T. S., Nair S. V., Tamura H.: Biomaterials based on chitin and chitosan in wound dressing applications. *Biotechnology Advances*, **29**, 322–337 (2011). <https://doi.org/10.1016/j.biotechadv.2011.01.005>
- [10] Negm N. A., Hefni H. H. H., Abd-Elaal A. A. A., Badr E. A., Abou Kana M. T. H.: Advancement on modification of chitosan biopolymer and its potential applications. *International Journal of Biological Macromolecules*, **152**, 681–702 (2020). <https://doi.org/10.1016/j.ijbiomac.2020.02.196>
- [11] Bakshi P. S., Selvakumar D., Kadirvelu K., Kumar N. S.: Chitosan as an environment friendly biomaterial – A review on recent modifications and applications. *International Journal of Biological Macromolecules*, **150**, 1072–1083 (2020). <https://doi.org/10.1016/j.ijbiomac.2019.10.113>
- [12] Shukla S. K., Mishra A. K., Arotiba O. A., Mamba B. B.: Chitosan-based nanomaterials: A state-of-the-art review. *International Journal of Biological Macromolecules*, **59**, 46–58 (2013). <https://doi.org/10.1016/j.ijbiomac.2013.04.043>
- [13] Khan Y. H., Islam A., Sarwar A., Gull N., Khan S. M., Munawar M. A., Zia S., Sabir A., Shafiq M., Jamil T.: Novel green nano composites films fabricated by indigenously synthesized graphene oxide and chitosan. *Carbohydrate Polymers*, **146**, 131–138 (2016). <https://doi.org/10.1016/j.carbpol.2016.03.031>
- [14] Yang X., Tu Y., Li L., Shang S., Tao X.-M.: Well-dispersed chitosan/graphene oxide nanocomposites. *ACS Applied Materials and Interfaces*, **2**, 1707–1713 (2010). <https://doi.org/10.1021/am100222m>
- [15] Wahba M. I.: Enhancement of the mechanical properties of chitosan. *Journal of Biomaterials Science, Polymer Edition*, **31**, 350–375 (2020). <https://doi.org/10.1080/09205063.2019.1692641>
- [16] Liu M., Zhang Y., Wu C., Xiong S., Zhou C.: Chitosan/halloysite nanotubes bionanocomposites: Structure, mechanical properties and biocompatibility. *International Journal of Biological Macromolecules*, **51**, 566–575 (2012). <https://doi.org/10.1016/j.ijbiomac.2012.06.022>
- [17] Wang S-F., Shen L., Zhang W-D., Tong Y-J.: Preparation and mechanical properties of chitosan/carbon nanotubes composites. *Biomacromolecules*, **6**, 3067–3072 (2005). <https://doi.org/10.1021/bm050378v>
- [18] Geim A. K.: Graphene: Status and prospects. *Science*, **324**, 1530–1534 (2009). <https://doi.org/10.1126/science.1158877>
- [19] Lee C., Wei X., Kysar J. W., Hone J.: Measurement of the elastic properties and intrinsic strength of monolayer graphene. *Science*, **321**, 385–388 (2008). <https://doi.org/10.1126/science.1157996>
- [20] Pan Y., Bao H., Li L.: Noncovalently functionalized multiwalled carbon nanotubes by chitosan-grafted reduced graphene oxide and their synergistic reinforcing effects in chitosan films. *ACS Applied Materials and Interfaces*, **3**, 4819–4830 (2011). <https://doi.org/10.1021/am2013135>
- [21] Kuila T., Bose S., Mishra A. K., Khanra P., Kim N. H., Lee J. H.: Chemical functionalization of graphene and its applications. *Progress in Polymer Science*, **57**, 1061–1105 (2012). <https://doi.org/10.1016/j.pmatsci.2012.03.002>

- [22] Zhang Y., Zhang M., Jiang H., Shi J., Li F., Xia Y., Zhang G., Li H.: Bio-inspired layered chitosan/graphene oxide nanocomposite hydrogels with high strength and pH-driven shape memory effect. *Carbohydrate Polymers*, **177**, 116–125 (2017).
<https://doi.org/10.1016/j.carbpol.2017.08.106>
- [23] Geng L., Lin Y., Chen S., Shi S., Cai Y., Li L., Peng X.: Superior strength and toughness of graphene/chitosan fibers reinforced by interfacial complexation. *Composites Science and Technology*, **194**, 108174 (2020).
<https://doi.org/10.1016/j.compscitech.2020.108174>
- [24] Huang Y., Zeng M., Chen J., Wang Y., Xu Q.: Multi-structural network design and mechanical properties of graphene oxide filled chitosan-based hydrogel nanocomposites. *Materials and Design*, **148**, 104–114 (2018).
<https://doi.org/10.1016/j.matdes.2018.03.055>
- [25] Zhang H-P., Luo X-G., Lin X-Y., Lu X., Tang Y.: The molecular understanding of interfacial interactions of functionalized graphene and chitosan. *Applied Surface Science*, **360**, 715–721 (2016).
<https://doi.org/10.1016/j.apsusc.2015.11.051>
- [26] Zhang H-P., Yang B., Wang Z. M., Xie C., Tang P., Bian L., Dong F., Tang Y.: Porous graphene oxide/chitosan nanocomposites based on interfacial chemical interactions. *European Polymer Journal*, **119**, 114–119 (2019).
<https://doi.org/10.1016/j.eurpolymj.2019.07.032>
- [27] Huang Q., Hao L., Xie J., Gong T., Liao J., Lin Y.: Tea polyphenol-functionalized graphene/chitosan as an experimental platform with improved mechanical behavior and bioactivity. *ACS Applied Materials and Interfaces*, **7**, 20893–20901 (2015).
<https://doi.org/10.1021/acsami.5b06300>
- [28] Layek R. K., Samanta S., Nandi A. K.: Graphene sulphonic acid/chitosan nano biocomposites with tunable mechanical and conductivity properties. *Polymer*, **53**, 2265–2273 (2012).
<https://doi.org/10.1016/j.polymer.2012.03.048>
- [29] Wrońska N., Anouar A., El Achaby M., Zawadzka K., Kędzierska M., Milowska K., Katir N., Draoui K., Różalska S., Piwoński I., Bryszewska M., El Kadib A., Lisowska K.: Chitosan-functionalized graphene nanocomposite films: Interfacial interplay and biological activity. *Materials (Basel)*, **13**, 998 (2020).
<https://doi.org/10.3390/ma13040998>
- [30] Wang J., Jin X., Li C., Wang W., Wu H., Guo S.: Graphene and graphene derivatives toughening polymers: Toward high toughness and strength. *Chemical Engineering Journal*, **370**, 831–854 (2019).
<https://doi.org/10.1016/j.cej.2019.03.229>
- [31] Wan S., Peng J., Li Y., Hu H., Jiang L., Cheng Q.: Use of synergistic interactions to fabricate strong, tough, and conductive artificial nacre based on graphene oxide and chitosan. *ACS Nano*, **9**, 9830–9836 (2015).
<https://doi.org/10.1021/acs.nano.5b02902>
- [32] Zhang J., Zou H., Qing Q., Yang Y., Li Q., Liu Z., Guo X., Du Z.: Effect of chemical oxidation on the structure of single-walled carbon nanotubes. *Journal of Physical Chemistry B*, **107**, 3712–3718 (2003).
<https://doi.org/10.1021/jp027500u>
- [33] Che J., Shen L., Xiao Y.: A new approach to fabricate graphene nanosheets in organic medium: Combination of reduction and dispersion. *Journal of Materials Chemistry*, **20**, 1722–1727 (2010).
<https://doi.org/10.1039/b922667b>
- [34] Hummers W. S., Offeman R. E.: Preparation of graphitic oxide. *American Chemical Society*, **208**, 1334–1339 (1958).
<https://doi.org/10.1021/ja01539a017>
- [35] Tu X., Luo X., Luo S., Yan L., Zhang F., Xie Q.: Novel carboxylation treatment and characterization of multi-walled carbon nanotubes for simultaneous sensitive determination of adenine and guanine in DNA. *Microchimica Acta*, **169**, 33–40 (2010).
<https://doi.org/10.1007/s00604-010-0307-3>
- [36] Liu Y., Deng R., Wang Z., Liu H.: Carboxyl-functionalized graphene oxide–polyaniline composite as a promising supercapacitor material. *Journal of Materials Chemistry*, **22**, 13619–13624 (2012).
<https://doi.org/10.1039/c2jm32479b>
- [37] Wang Z., Dong Y., Li H., Zhao Z., Wu H. B., Hao C., Liu S., Qiu J., Lou X. W.: Enhancing lithium-sulphur battery performance by strongly binding the discharge products on amino-functionalized reduced graphene oxide. *Nature Communications*, **5**, 5002 (2014).
<https://doi.org/10.1038/ncomms6002>
- [38] Park K-W.: Carboxylated graphene oxide-Mn₂O₃ nanorod composites for their electrochemical characteristics. *Journal of Materials Chemistry A*, **2**, 4292–4298 (2014).
<https://doi.org/10.1039/C3TA14223J>
- [39] Navaee A., Salimi A.: Efficient amine functionalization of graphene oxide through the bucherer reaction: An extraordinary metal-free electrocatalyst for the oxygen reduction reaction. *RSC Advances*, **5**, 59874–59880 (2015).
<https://doi.org/10.1039/c5ra07892j>
- [40] Ding L., Huang Y., Cai X., Wang S.: Impact of pH, ionic strength and chitosan charge density on chitosan/casein complexation and phase behavior. *Carbohydrate Polymers*, **208**, 133–141 (2019).
<https://doi.org/10.1016/j.carbpol.2018.12.015>
- [41] Cobos M., González B., Fernández M. J., Fernández M. D.: Chitosan-graphene oxide nanocomposites: Effect of graphene oxide nanosheets and glycerol plasticizer on thermal and mechanical properties. *Journal of Applied Polymer Science*, **134**, 45092 (2017).
<https://doi.org/10.1002/app.45092>

- [42] Rodríguez-González C., Martínez-Hernández A. L., Castaño V. M., Kharissova O. V., Ruoff R. S., Velasco-Santos C.: Polysaccharide nanocomposites reinforced with graphene oxide and keratin-grafted graphene oxide. *Industrial and Engineering Chemistry Research*, **51**, 3619–3629 (2012).
<https://doi.org/10.1021/ie200742x>
- [43] Dhayal V., Hashmi S. Z., Kumar U., Choudhary B. L., Kuznetsov A. E., Dalela S., Kumar S., Kaya S., Dolia S. N., Alvi P. A.: Spectroscopic studies, molecular structure optimization and investigation of structural and electrical properties of novel and biodegradable chitosan-GO polymer nanocomposites. *Journal of Materials Science*, **55**, 14829–14847 (2020).
<https://doi.org/10.1007/s10853-020-05093-5>
- [44] Wang Y., Shi Z., Yin J.: Facile synthesis of soluble graphene *via* a green reduction of graphene oxide in tea solution and its biocomposites. *ACS Applied Materials and Interfaces*, **3**, 1127–1133 (2011).
<https://doi.org/10.1021/am1012613>
- [45] Wang X., Bai H., Yao Z., Liu A., Shi G.: Electrically conductive and mechanically strong biomimetic chitosan/reduced graphene oxide composite films. *Journal of Materials Chemistry*, **20**, 9032–9036 (2010).
<https://doi.org/10.1039/C0JM01852J>
- [46] Lu Y., Fan L., Yang L-Y., Huang F., Ouyang X-K.: PEI-modified core-shell/bead-like amino silica enhanced poly(vinyl alcohol)/chitosan for diclofenac sodium efficient adsorption. *Carbohydrate Polymers*, **229**, 115459 (2020).
<https://doi.org/10.1016/j.carbpol.2019.115459>
- [47] Cheng Q., Jiang L., Tang Z.: Bioinspired layered materials with superior mechanical performance. *Accounts of Chemical Research*, **47**, 1256–1266 (2014).
<https://doi.org/10.1021/ar400279t>